Predicting the permeability and tensile behavior of high density polyethylene/tie/polyamide 6 three-layer films

Chi-Hsien Huang,[1] Jiann-Shing Wu[1]* and Chun-Chin Huang[2]

[1]*Department of Applied Chemistry, National Chiao Tung University, 1001 Ta Hsueh Road, Hsinchu 30043, Taiwan*
[2]*Department of Mold and Die Engineering, National Kaohsiung University of Applied Science, Kaohsiung 807, Taiwan*

Abstract: Multilayer films with multiple properties have been widely applied in the packaging industry. In order to know the two most important properties, *ie* permeability and tensile property, of the multilayer films, we examined model predictions and the properties of the individual component layers to provide an efficient method to design desired multilayer structures. The series model was employed for predicting permeability; there is good agreement between experimental data and this model for predicting both gas and water vapor permeabilities of three-layer films with various thickness fractions of polyamide 6 (PA-6). We can also predict the parameters of the constitutive equation, which described the plastic deformation of the three-layer films, from those of the individual component layers, with particularly high accuracy by using the additive rule. However, there was a larger discrepancy between the model and experimental data at high crosshead speeds due to the generation of heat during deformation.
© 2004 Society of Chemical Industry

Keywords: coextrusion; multilayer; plastic deformation; permeability

INTRODUCTION

It is common to introduce multilayer structures comprising different polymers to form a product with multiple properties. Each property takes advantage of the best property of each individual component. A multilayer extruded product can be produced by coextrusion into the various types of multilayer sheets, blown films, cast films, tubing, and containers.[1–5]

Polyethylene (PE) and polyamide 6 (PA-6) are two important classes of polymers used in coextrusion that are very popular in the packaging industry. PE is widely employed because of its low cost, easy processibility, chemical inertness and high moisture barrier properties, but its poor barrier properties against oxygen, aromas and organic solvents limit its applications.[6–9] On the other hand, PA-6 is a good barrier resin against oxygen, aromas and organic solvents and it has high tensile strength and toughness, but it is relatively expensive and a poor barrier against water vapor.[10–13] For packaging applications, it is reasonable to combine these two resins into a single structure by using a coextrusion process to form multilayer films with multiple properties. An extrudable adhesive is often incorporated into the multilayer structure as a tie layer in the coextrusion process due to the incompatibility between these two polymers. Kamykowski[14] studied the adhesive properties of five-layer polypropylene/adhesive/polyamide/adhesive/polypropylene co-extruded cast films and found that adhesion can be generally improved by increasing the overall film thickness or the relative amount of the adhesive. Homopolymer diluents in the adhesive layer have better adhesion properties than random copolymers. The molecular weight of the grafted polymer of adhesive has a small effect on adhesion. By combining graft and polymer blending, Tanaka *et al*[15] have successfully developed a new generation of tie layer adhesives that maintain high adhesive strengths after thermoforming and orientation. A blend of component material and adhesive as both the adhesion-promoting layer and support layer was used to eliminate the tie layer and provide adhesion between the chemically dissimilar layers,[16–18] *eg* the five-layer film coextrusion system was replaced with a three-layer film comprising ethylene-vinyl alcohol copolymer (EVOH) as the central layer and low density polyethylene/low density polyethylene grafted maleic anhydride (LDPE/LDPE-*g*-MAH) blends as the external layers to form a three-layer structure, A/B/A (blend/EVOH/blend).[18]

In packaging applications, the permeability and tensile strength are the two most important properties. These two properties of monolayers of high density polyethylene (HDPE) and PA-6 have been reported in

previous literature[13,19−23] with the aim of constructing a method for effectively predicting the specific properties of a multilayer structure from the properties of its individual component materials. In this paper we use a three-layer film, HDPE/tie/PA-6, to examine the permeabilities of nitrogen (N_2), oxygen (O_2), carbon dioxide (CO_2) and water vapor and the tensile properties of three-layer films fabricated *via* a coextruded blown-film process using a series model[24] and an additive rule[25] as predicting methods, respectively. The aim of the study is to provide an economical and efficient tool for designing the compositions of the multilayer sheets, films and containers to achieve the desired properties by coextrusion.

EXPERIMENTAL
Materials
The materials used in the coextrusion blown-film process were high density polyethylene (HDPE), polyamide-6 (PA-6) and adhesive, high density polyethylene grafted maleic anhydride (HDPE-*g*-MAH). HDPE was supplied in pellet form by Formosa Plastic Corp (Taiwan): HDPE 9001 with melt index 0.05 g (10 min)$^{-1}$ (190 °C, 2.16 kg) and density of 0.95 g cm^{-3}. The PA-6 was provided in pellet form by Mitsubishi Engineering Plastic Co. (Japan): Novamid 1030 with melt index of 5 g (10 min)$^{-1}$ (240 °C, 2.16 kg) and density of 0.95 g cm^{-3}. The adhesive was obtained in pellet form from Mitsubishi Chemical Corp. (Japan): Modic-AP H503 with melt index of 1.5 g (10 min)$^{-1}$ (190 °C, 2.16 kg) and density of 0.93 g cm^{-3}.

Preparation of multilayer films
Because of the hydrophilic property of PA-6, the polymer was dried in a vacuum oven for 12 h at 90 °C before processing. HDPE, PA-6, and HDPE-*g*-MAH were fed separately into their individual extruders and coextruded through a three-layer coextrusion blown-film die (inner diameter = 97.6 mm; gap thickness = 1.2 mm) at 250 °C. The three-layer film was inflated and cooled with air and stretched by a take-up device after leaving the exit of the die. Monolayers of PA-6 and HDPE films were also prepared using the same blown-film equipment. All samples were placed in a cabinet for 14 days maintained at 25 °C. Four different compositions of the component layers were prepared and the overall thickness of three-layer multilayered films was *ca* 140 μm. Table 1 presents the thicknesses and thickness fractions of the PA-6 layers; the compositions of all the three-layer films were controlled by using gear pumps precisely and steadily and the individual thicknesses of the component layers were measured by using ultrasonic thickness measurement (Quinsonic, ElektroPhysik). Because the tie layer generally was very thin (*ca* 5 μm in this study) in the coextrusion process, and the main molecular structure was HDPE, we consider the tie

Table 1. Thickness and thickness fraction of PA-6 layer in three-layer films

Thickness (μm)	Thickness fraction (%)
14	10
28	20
42	30
63	45

layer to be part of the HDPE layer and neglect its effect on permeability and tensile behavior in this study.

Permeability measurement
The gas permeability, including that towards nitrogen (N_2), oxygen (O_2) and carbon dioxide (CO_2), was measured using a Lyssy L-100-5000 gas permeability tester,[26] following ASTM Standard Method D1434. The gas permeability of the samples was measured at 23 °C and a relative humidity of 0 %. Water vapor permeability was measured using a Lyssy L-80-5000 water vapor permeability tester,[27] following ASTM Standard Method E96. The water vapor permeability of the samples was measured at 38 °C and a relative humidity of 90 %. The temperatures of both measurements were controlled by a water bath. Measurements were taken on five replicate samples; average values are reported.

Tensile behavior measurement
The uniaxial tensile behavior of test samples with dimension of 40 mm length and 20 mm width were measured by using a Hung-Ta instrument model 2102AP. Three crosshead speeds, 4, 40 and 400 mm min^{-1}, were employed to test samples at a temperature of 25 °C and a relative humidity of 50 %. Engineering stress−strain curves were determined from load-displacement data based on the original geometry of the test samples. Measurements were taken on five replicate samples.

We calculated the engineering stress and strain by employing the original geometry of the sample film, but the cross-sectional area of the film sample changed continuously during actual deformation. So, the engineering stress and strain cannot represent the actual stress and strain at any instant during deformation. It is necessary and more instructive to plot the true stress−strain curves to describe the tensile behavior. If the test sample deformed homogeneously, the constancy of volume was assumed during deformation and the true strain, ε_T, and the true stress, σ_T, were calculated by

$$\varepsilon_T = \ln(1 + \varepsilon_E) \qquad (1)$$

$$\sigma_T = \sigma_E(1 + \varepsilon_E) \qquad (2)$$

where ε_E and σ_E are the engineering strain and the engineering stress, respectively.[19,28] On the other hand, if the deformation was inhomogeneous, *ie*, a neck formed, the surface of each sample film

Table 2. Gas Permeabilities of monolayer PA-6, monolayer HDPE and three-layer films

Thickness fraction of PA-6 layer (%)	Permeability ($\mathrm{ml\,mm\,m^{-2}\,day^{-1}\,atm^{-1}}$)		
	N_2	O_2	CO_2
0 (HDPE)	1.26	9.28	17.41
10	1.21	6.73	16.20
20	1.07	4.61	13.22
30	0.87	4.10	12.66
45	0.82	2.94	10.37
100 (PA-6)	0.55	1.73	7.50

was marked with a set of 199 points, which were positioned 0.2 mm apart along the 40 mm gauge length of the specimen before testing.[29] The evolution of the specimen profile during a test was recorded continuously with the aid of a CCD video camera that was coupled with a microscope mounted on a screw-driven device and connected to a computer. The true stress and strain were determined by measuring the local deformation in the neck region from photographs obtained by a frame grabber during the experiment. Assuming that the sample retained constant volume during deformation, the true stress and true strain were calculated by

$$\varepsilon_{T} = \ln(1 + \varepsilon_{L}) \qquad (3)$$

$$\sigma_{T} = \sigma_{eng}(1 + \varepsilon_{L}) \qquad (4)$$

where ε_{L} is the longitudinal strain of the displacement between two markers in the neck region. These markers were monitored along the central axis and the cross-section of sample was rectangular so that the effect of triaxiality during necking could be ignored.[29,30]

RESULTS AND DISCUSSION
Permeability
Table 2 lists the gas permeabilities of PA-6 and HDPE films. The PA-6 film has much better barrier properties than HDPE toward all these gases, with permeabilities for both films increasing in the order $CO_2 > O_2 > N_2$. Table 2 also displays the gas permeabilities of three-layer films with various thickness fractions of the PA-6 layer. The values of gas permeabilities of these three-layer films all lie between those of the individual component layers for all the gases. As expected, the permeability toward all gases decreased upon increasing the thickness fraction of the PA-6 layer. In order to predict the gas permeability of a three-layer film from that of its individual component layers, we employed a series model[24] because of the lamellar structure of these films.

$$\frac{1}{P_{M}} = \frac{L_{HDPE}}{P_{HDPE}} + \frac{L_{PA-6}}{P_{PA-6}} \qquad (5)$$

where P_{M} is the permeability of the three-layer film, P_{HDPE} and P_{PA-6} are the permeabilities of the monolayer films of HDPE and PA-6, respectively, and L_{HDPE} and L_{PA-6} are the thickness fractions of HDPE (including the tie layer) and PA-6 in the three-layer films, respectively. The gas permeabilities of three-layer films toward N_2, O_2, and CO_2 are presented in Figs 1, 2 and 3, respectively, for both the series model and the experimental data. There is good agreement between the model's predictions and the experimental data for all these gases.

Table 3 lists the water vapor permeabilities of HDPE and PA-6 films. In contrast to the gas permeabilities, we see that the HDPE film has a much better water vapor barrier property than that of PA-6. Table 3 also presents the water vapor permeabilities of the three-layer films as a function of the thickness fraction of the PA-6 layer. Similarly to the gas permeabilities, the values of water vapor permeabilities all lie between those of the individual component layers. Fig 4 displays the water vapor permeabilities of the three-layer films as a function of the thickness fraction of the PA-6 layer. For the sake of comparison, this figure also presents the predictions
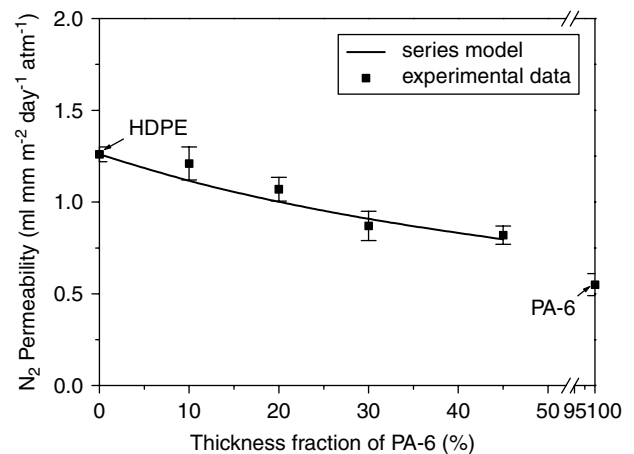
Figure 1. Nitrogen (N_2) permeabilities of three-layer films with various contents of PA-6.
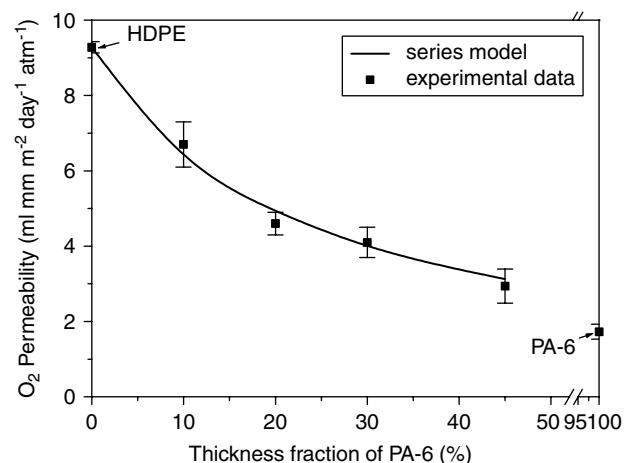
Figure 2. Oxygen (O_2) permeabilities of three-layer films with various contents of PA-6.
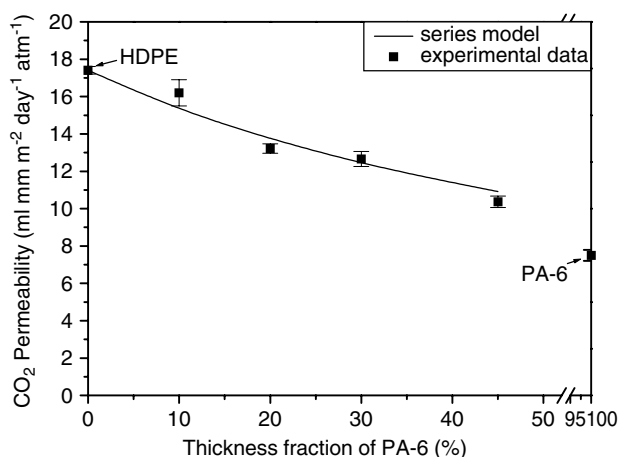
Figure 3. Carbon dioxide (CO_2) permeabilities of three-layer films with various contents of PA-6.

Table 3. Water vapor permeabilities of monolayer PA-6, monolayer HDPE and three-layer films

Thickness fraction of PA-6 layer (%)	Permeability ($g\,mm\,m^{-2}\,day^{-1}$)
0 (HDPE)	2.71
10	2.82
20	3.53
30	4.00
45	5.01
100 (PA-6)	987.52
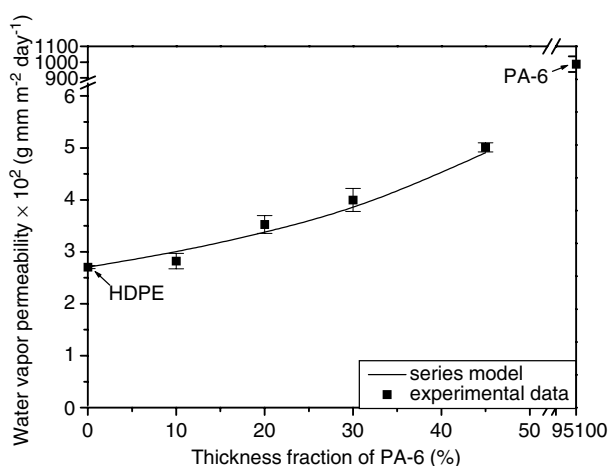
**Figure 4.** Water vapor permeabilities of three-layer films with various contents of PA-6.

obtained by the model using Eqn (5). The water vapor permeabilities increase with increasing PA-6 content and agree reasonably well with the series model.

Tensile behavior

The engineering stress–strain curves for the monolayer films of HDPE and PA-6 are presented in Fig 5. We see that the HDPE film deforms inhomogeneously at these three crosshead speeds, 4, 40 and 400 mm min^{-1}. A significant load drop can be seen to occur, which is associated with stable neck formation at the central cross-section. The load drop is followed
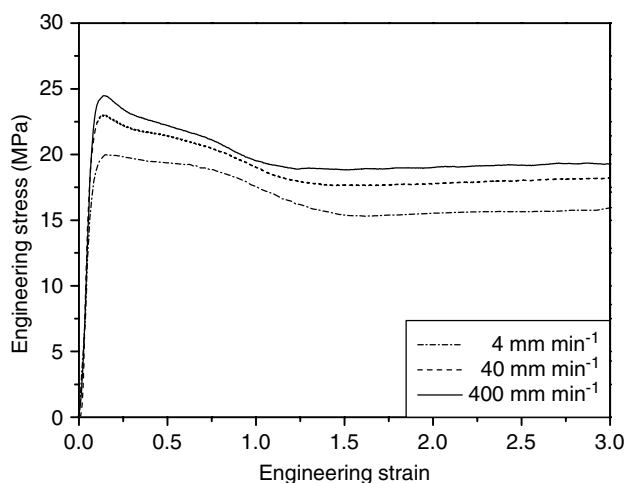
(a)
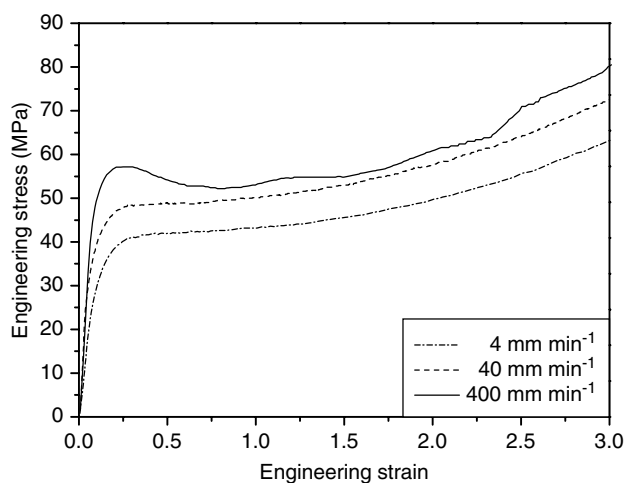
(b)

Figure 5. Engineering stress–strain curves of (a) HDPE and (b) PA-6 films at various crosshead speeds.

by cold drawing, which is associated with neck propagation along the specimen. The true stress–strain curve was determined by measuring the local strain during neck region and applying Eqns (3) and (4). On the other hand, the PA-6 film shows obviously different tensile behavior compared to HDPE films. The PA-6 film exhibits a higher level of engineering stress and deforms homogeneously at low level of crosshead speeds, ie 4 and 40 mm min^{-1}. At higher level of strain, the engineering stress increases rapidly with the increase of engineering strain due to the molecular alignment;[31] this effect is known as strain hardening. The true stress–strain curve was calculated using Eqns (1) and (2). However, at the high level of crosshead speed, ie 400 mm min^{-1}, the deformation mode changes from homogeneous to inhomogeneous and the true stress–strain curve was determined as for HDPE. Fig 6 displays the true stress–strain curves of the PA-6 and HDPE films.

To model the deformation behavior of the films, we employed the following empirical constitutive equation:[19,32]

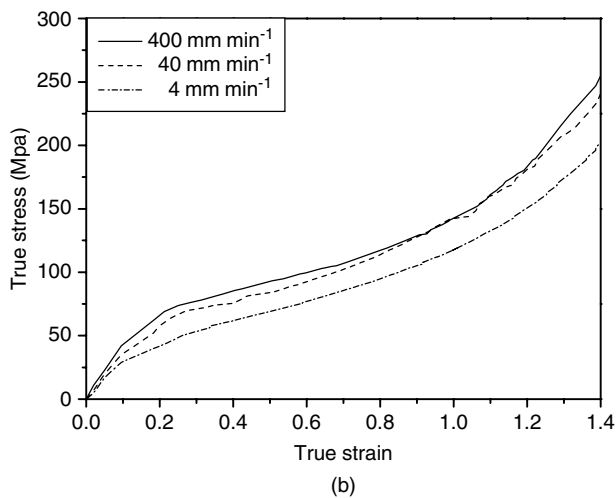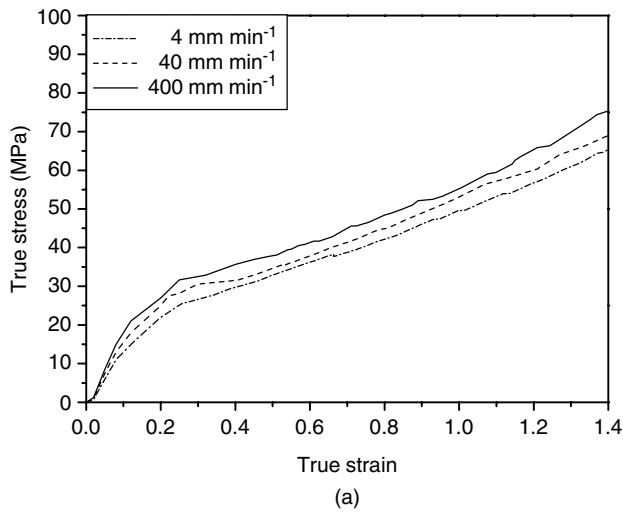$$\sigma = \sigma_0 \exp(\gamma \cdot \varepsilon_T) \tag{6}$$

Figure 6. True stress–strain curves of (a) HDPE and (b) PA-6 films at various crosshead speeds.

where σ_0 and γ are the true yield stress and the strain hardening parameter, respectively. The constitutive equation can also be presented in the following form:

$$\ln \sigma = \ln \sigma_0 + \gamma \cdot \varepsilon_\mathrm{T} \qquad (7)$$

From Eqn (7), the relationship of the natural logarithm of true stress ($\ln \sigma$) and true strain (ε_T) should be linear in the region of plastic deformation. In a least-squares approximation to the plot of $\ln \sigma$ *versus* ε_T, the slope and intercept correspond to the strain hardening parameter (γ) and the natural logarithm of the true yield stress ($\ln \sigma_0$), respectively. Fig 7 displays the fitted curves and experimental data of the $\ln \sigma$ *versus* ε_T for the HDPE and PA-6 films. A linear relationship for both films appears to exist over the range of true strains from 0.25 to 1.40 with the correlation coefficients all >0.99 with respect to the approximation. The corresponding parameters of the constitutive equation for the HDPE and PA-6 films at various crosshead speeds are summarized in Table 4. For comparison, Fig 8 displays both the experimental true stress–strain data and the modeling curves. Good agreement exists between the modeling curves and
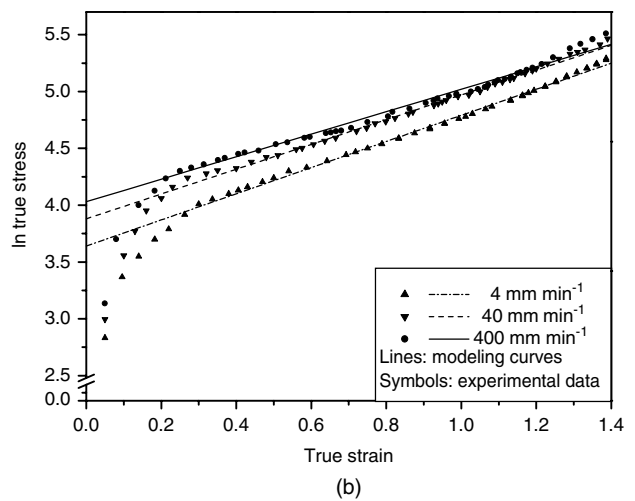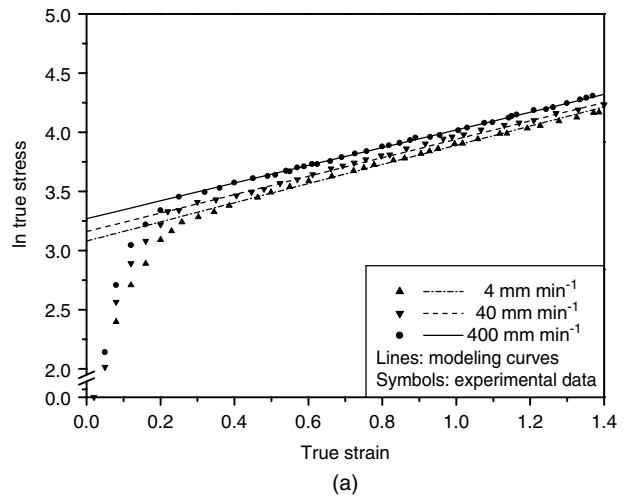

Figure 7. Modeling and experimental data of ln true stress strain of *versus* true (a) HDPE and (b) PA-6 films at various crosshead speeds.

Table 4. True yield stress (σ_0) and strain hardening parameter (γ) of HDPE, PA-6 and three-layer films at various crosshead speeds

Thickness fraction of PA-6 layer (%)	Crosshead speed (mm min^{-1})					
	4		40		400	
	σ_0 (MPa)	γ	σ_0 (MPa)	γ	σ_0 (MPa)	γ
0 (HDPE)	21.54	0.80	23.57	0.78	26.20	0.75
10	22.20	0.87	25.79	0.86	27.66	0.78
20	24.78	0.91	27.66	0.89	30.88	0.81
30	25.66	0.97	30.88	0.92	34.47	0.84
45	29.67	1.02	33.78	0.97	38.09	0.86
100 (PA-6)	38.09	1.15	48.43	1.10	55.70	0.99

experimental data for the range of plastic deformation of the HDPE and PA-6 films.

Fig 9 presents a plot of the engineering and true stress–strain curves of three-layer films with various thickness fractions of PA-6 at a crosshead speed of $40 \, \mathrm{mm \, min^{-1}}$. It is clear that these curves all lie between those obtained for monolayers of HDPE and PA-6 films. The stress level increases with increasing thickness fraction of the PA-6 layer and, in addition, the strain hardening behavior due to the molecular alignment becomes more obvious. In the range of
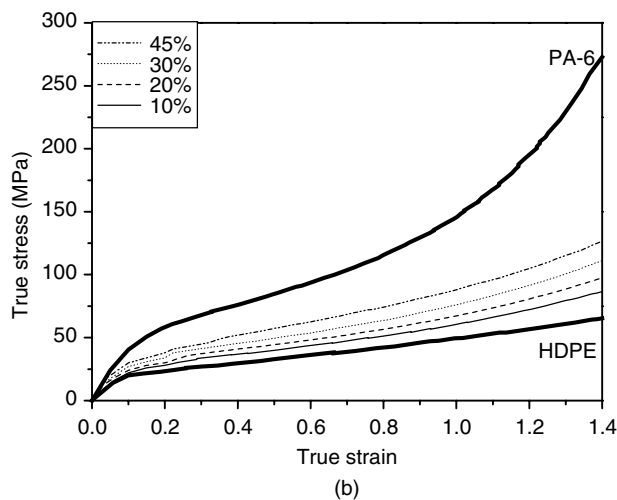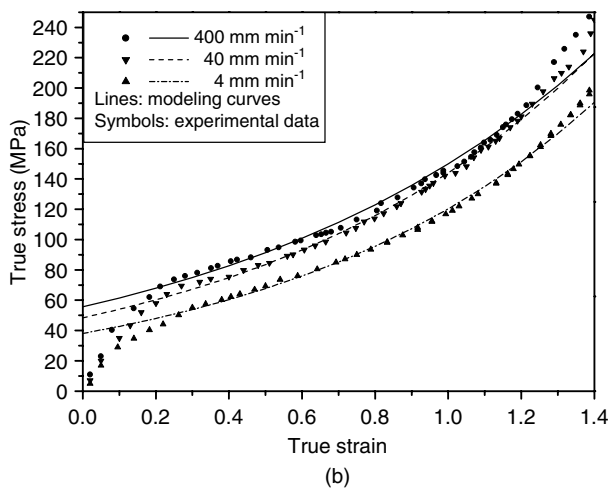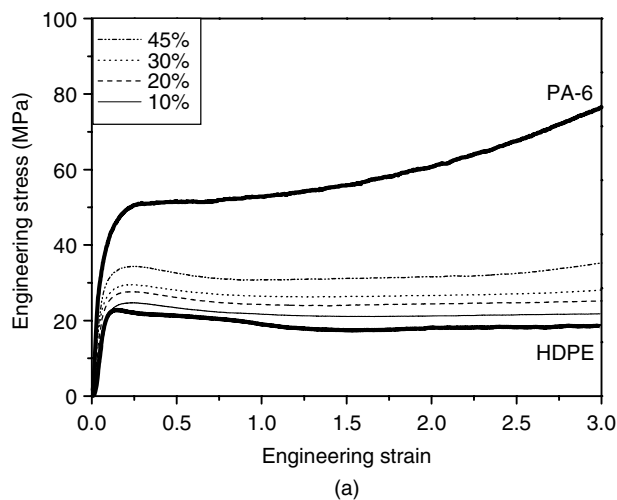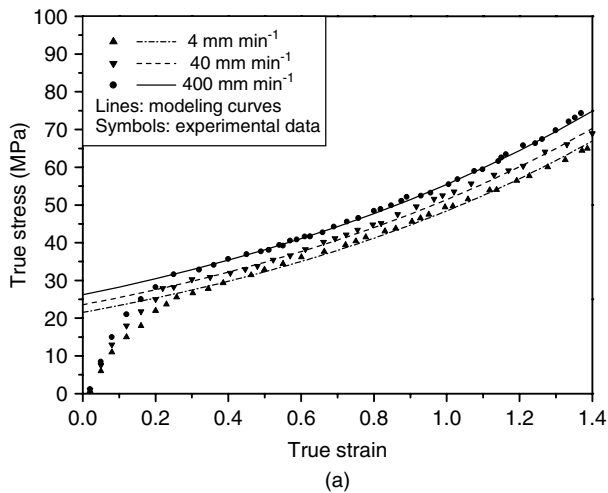
Figure 8. Comparison of true stress–strain curves between modeling curves and experimental data of (a) HDPE and (b) PA-6 films at various crosshead speeds.

Figure 9. Stress–strain curves of three-layer films as a function of thickness fraction of PA-6 layer at crosshead speed 40 mm min^{-1}. The thick solid lines represent the PA-6 and HDPE monolayers. (a) Engineering; (b) True.

thickness fractions of PA-6 that we investigated, all the three-layer films deform inhomogeneously at this crosshead speed. A linear relationship also appears to exist for the three-layer films over the same range of true strains (0.25–1.40) as it did for the HDPE and PA-6 films at crosshead speed 40 mm min^{-1}. The correlation coefficients are also all >0.99 with respect to the approximation. The corresponding parameters of the constitutive equation for the three-layer films at various crosshead speeds are also listed in Table 4. A comparison of the modeling curves and experimental true stress–strain data at crosshead speed 40 mm min^{-1} is shown in Fig 10. There is also good agreement between the experimental data and the modeling curves over the range of plastic deformation for the three-layer films with various thickness fractions of PA-6.

Similarly to what we reported above for predicting permeability, we introduced a simple theoretical additive rule model[25] to predict the tensile behavior of a three-layer film from those of its individual component layers:

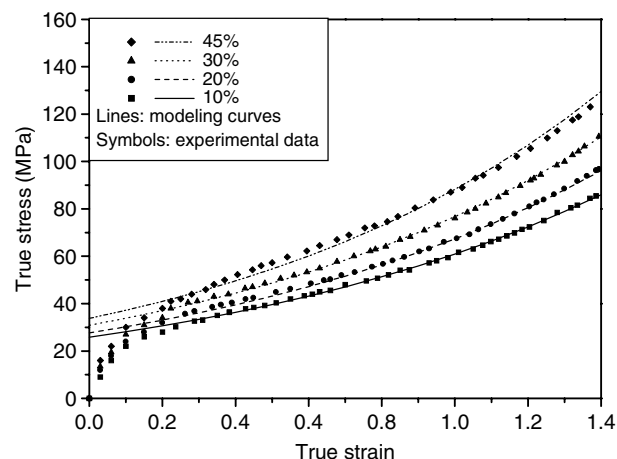$$\sigma_M = L_{HDPE}\,\sigma_{HDPE} + L_{PA-6}\,\sigma_{PA-6} \qquad (8)$$

Figure 10. Comparison of true stress–strain curves between modeling curves and experimental data of three-layer films as a function of thickness fraction of PA-6 layer at crosshead speed 40 mm min^{-1}.

where σ_M is the true stress of a three-layer film, σ_{HDPE} and σ_{PA-6} are the true stresses of the HDPE and PA-6 layers, respectively, and L_{HDPE} and L_{PA-6} are the

thickness fractions of HDPE (including the tie layer) and PA-6 layers, respectively.

From Eqns (6) and (8), the relationship between the true stress–strain of the three-layer and the individual component layer films is

$$\sigma_{0M} \exp(\gamma_M \cdot \varepsilon_T) = L_{PA-6}\, \sigma_{0PA-6} \exp(\gamma_{PA-6} \cdot \varepsilon_T)$$
$$+ L_{HDPE}\, \sigma_{0HDPE} \exp(\gamma_{HDPE} \cdot \varepsilon_T) \qquad (9)$$

where σ_{0M} is the true yield stress of the three-layer film, σ_{0HDPE} and σ_{0PA-6} are the true yield stresses of the HDPE and PA-6 layers, respectively, and γ_M, γ_{HDPE} and γ_{PA-6} are the strain hardening parameters of the three-layer film, HDPE, and PA-6 layers, respectively. It is reasonable to assume that the true yield stress of the three-layer film alone follows the additive rule:

$$\sigma_{0M} = L_{PA-6}\sigma_{0PA-6} + L_{HDPE}\sigma_{0HDPE} \qquad (10)$$

and the strain hardening parameter of the three-layer film is defined as[33]

$$\gamma_M(\varepsilon) = \frac{\partial \ln \sigma_M}{\partial \varepsilon}$$
$$= \frac{\partial [L_{PA-6}\sigma_{0PA-6} \exp(\gamma_{PA-6} \cdot \varepsilon) + L_{HDPE}\sigma_{0HDPE} \exp(\gamma_{HDPE} \cdot \varepsilon)]}{\partial \varepsilon} \qquad (11)$$

We calculated the parameters σ_{0M} and γ_M for the additive rule by using the parameters of the individual component layers in Table 4. Figures 11 and 12 present the dependence of these parameters obtained by the additive rule and the experimental data (from Table 4) with respect to the compositions of films. We can see that good agreement exists between the experimental data and the additive-rule model for both the strain hardening parameter and true yield stress at low crosshead speeds, which suggests that this rule can be used to accurately predict the plastic deformation of the three-layer films. However, a larger discrepancy existed between the model and experimental data at high crosshead speed for both these parameters of the three-layer films. This is due to the generation of heat during deformation,[34] which causes a decrease in the stress to produce a given strain.

CONCLUSIONS

In this study we have successfully fabricated HDPE/tie/PA-6 three-layer films, a typical multilayer A/B/C structure, by a coextrusion blown-film process. We have investigated N_2, O_2, CO_2 and water vapor permeabilities. We found that predicting both the gas and water vapor permeability of the three-layer films with respect to the thickness fraction of PA-6 based upon those of the individual component layer films is in good agreement with the experimental data when using the series model. On the other hand, a constitutive equation was employed to describe the tensile
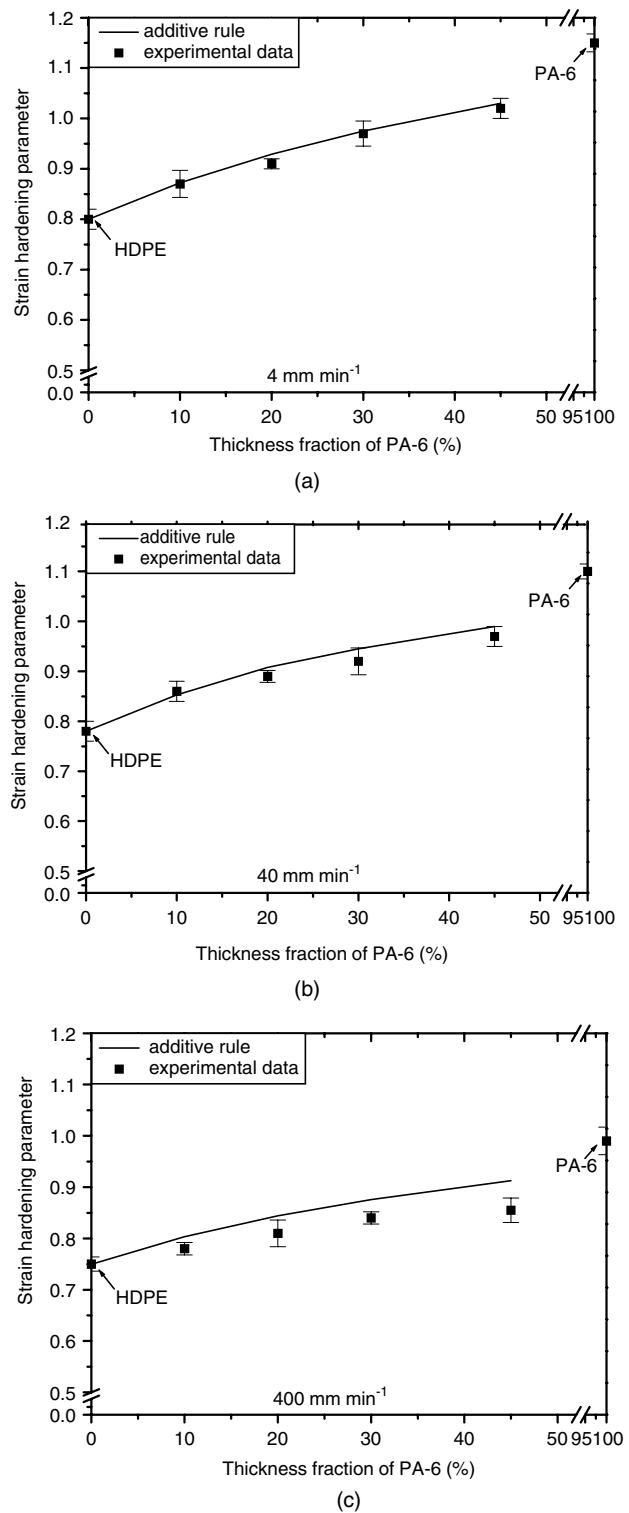

Figure 11. Comparison of strain hardening parameter between additive rule and experimental data as a function of PA-6 content at various crosshead speeds: (a) 4 mm min^{-1}; (b) 40 mm min^{-1}; (c) 400 mm min^{-1}.

behavior of the films over the range of plastic deformation. The tensile behavior of the component layer and multilayer films at various crosshead speeds can be precisely expressed by a constitutive equation having two parameters in the true stress–strain relationship, ie, the true yield stress and the strain hardening parameter.
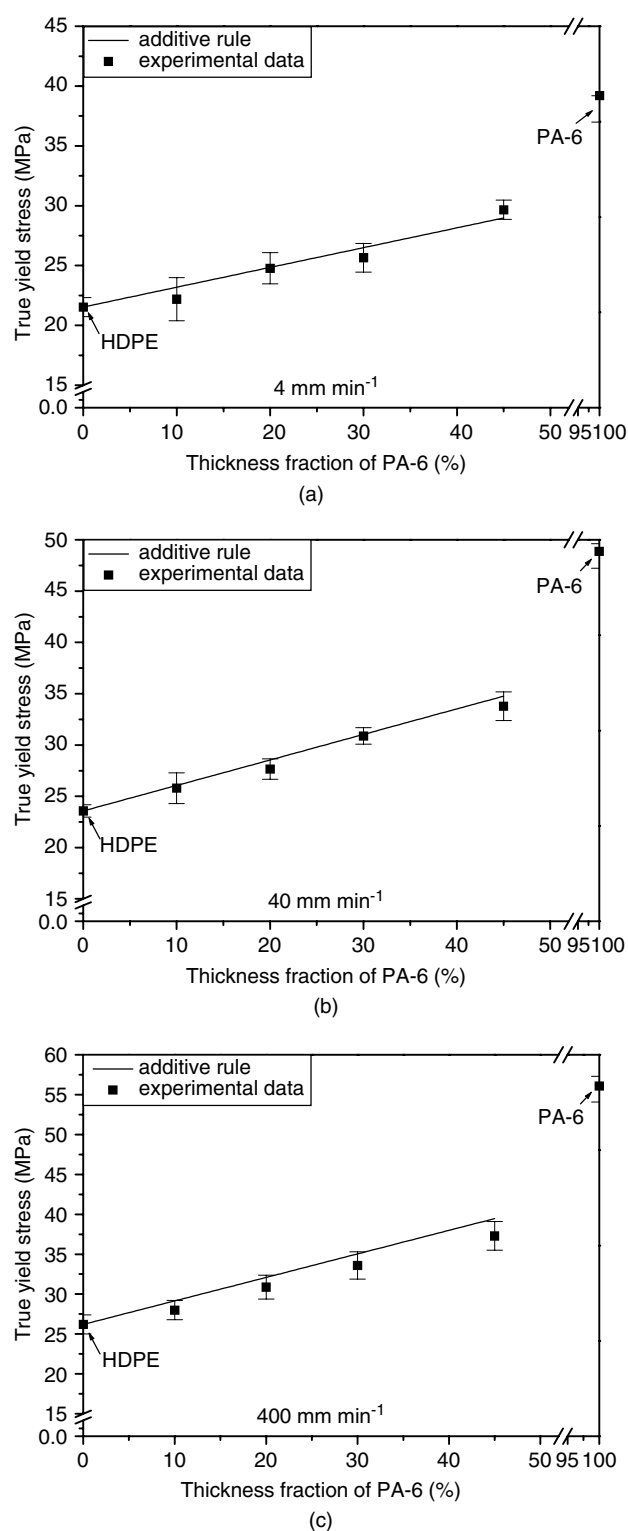
Figure 12. Comparison of true yield stress between additive rule and experimental data as a function of PA-6 content at various crosshead speeds: (a) 4 mm min^{-1}; (b) 40 mm min^{-1}; (c) 400 mm min^{-1}.

We examined the relationships between the parameters of the monolayers of the component layers and those of the three-layer films by using an additive rule. This could predict the tensile properties, including the

true yield stress and strain hardening, of the three-layer films from those of the individual component layers with good agreements in the true stress–strain relationship. However, there was a larger discrepancy between the model and experimental data at high crosshead speed due to the generation of heat during deformation.

In summary, we could efficiently design the compositions of the multilayer structure to achieve specific permeability and/or tensile properties by employing these model predictions before processing.

REFERENCES

1 Culter J, Krohn J and Todd W, *Pack Tech Eng* **8**:30 (1999).
2 Dooley J, Hyun KS and Hughes K, *Polym Eng Sci* **38**:1060 (1998).
3 Schrenk WJ and Marcus SA, *J Plast Film Sheet* **1**:30 (1985).
4 Hosoda S, Seki Y and Kihara H, *Polymer* **34**:4602 (1993).
5 Liu SJ and Yang CH, *Adv Polym Tech* **20**:108 (2001).
6 Hensen F, *Plastics Extrusion Technology*, Hanser, New York, Chapter 5 (1997).
7 Rubin II, *Handbook of Plastic Materials and Technology*, Wiley, New York, Chapter 30 (1990).
8 Sabne MB, Thombre SM, Patil AS, Patil SD, Idage SB and Vernekar SP, *J Appl Polym Sci* **58**:1275 (1995).
9 Gill TS and Xanthos M, *Polym Eng Sci* **2**:248 (1996).
10 Climenhage DC, *Packaging* **32**:39 (1987).
11 Eichler S and Miltz J, *J Appl Polym Sci* **50**:2095 (1993).
12 Rubin II, *Handbook of Plastic Materials and Technology*, Wiley, New York, Chapter 16 (1990).
13 Khanna YP, Day ED, Tsai ML and Vaidyanathan G, *J Plast Film Sheet* **13**:197 (1997).
14 Kamykowski GW, *J Plast Film Sheet* **16**:237 (2000).
15 Tanaka H, Shigemoto H and Kawchi H, *J Plast Film Sheet* **12**:279 (1996).
16 Valdes SS, Villarreal FO, Quintanilla ML, Flores IY and Ramos de Valle LF, *Polym Eng Sci* **38**:127 (1998).
17 Olmos JV, Valdes SS and Yánez Flores IG, *Polym Eng Sci* **39**:1597 (1999).
18 Huang CH, Wu JS, Huang CC and Lin LS, *Polym J* **35**:978 (2003).
19 Bahadur S, *Polym Eng Sci* **13**:266 (1973).
20 Wang Y, Easteal AJ and Chen XD, *Pack Tech Sci* **11**:169 (1998).
21 Lin L and Argon AS, *J Mater Sci* **29**:294 (1994).
22 Bianchi S, Cantagallo S, Consolati G, Laporta M, Pegoraro M, Tieghi G and Zanderighi L, *J Appl Polym Sci* **86**:559 (2002).
23 Lin L and Argon AS, *J Mater Sci* **29**:294 (1994).
24 Faisant JB, Aït-Kadi A, Bousmina M and Deschênes L, *Polymer* **39**:533 (1998).
25 Schrenk WJ and Alfrey T, *Polym Eng Sci* **9**:393 (1969).
26 *Automatic Manometric Gas Permeability Tester Operator Manual, Model L100-5000*, Lyssy AG (2001).
27 *Automatic Manometric Water Vapor Permeability Tester Operator Manual, Model L80-5000*, Lyssy AG (2001).
28 Al-Hussein M and Strobl G, *Macromolecules* **35**:8515 (2002).
29 G'Sell C, Aly-Helal NA and Jonas JJ, *J Mater Sci* **18**:1731 (1983).
30 Gěrard Buisson and Ravi-Chandar K, *Polymer* **31**:2071 (1990).
31 Peterlin A, *J Mater Sci* **6**:490 (1971).
32 Gaucher-Miri V, Jones GK, Kaas R, Hiltner A and Baer E, *J Mater Sci* **37**:2635 (2002).
33 Hart EW, *Acta Metall* **15**:351 (1967).
34 Hall IH, *J Appl Polym Sci* **12**:739 (1968).